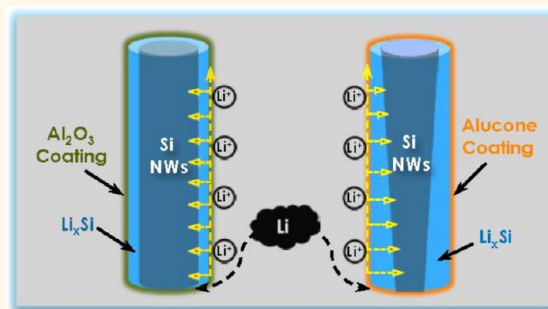


Surface-Coating Regulated Lithiation Kinetics and Degradation in Silicon Nanowires for Lithium Ion Battery

Langli Luo,^{†,¶} Hui Yang,^{*,¶} Pengfei Yan,[†] Jonathan J. Travis,[§] Younghee Lee,[§] Nian Liu,^{||} Daniela Molina Piper,[§] Se-Hee Lee,[§] Peng Zhao,[‡] Steven M. George,[§] Ji-Guang Zhang,[⊥] Yi Cui,^{||,¶} Sulin Zhang,^{*,‡} Chunmei Ban,^{*,∇} and Chong-Min Wang^{*,†}

[†]Environmental Molecular Sciences Laboratory, Pacific Northwest National Laboratory, 902 Battelle Boulevard, Richland, Washington 99352, United States, [‡]Engineering Science and Mechanics and Bioengineering, Pennsylvania State University, University Park, Pennsylvania 16802, United States, [§]University of Colorado at Boulder, Boulder, Colorado 80309, United States, ^{||}Department of Materials Science and Engineering, Stanford University, Stanford, California 94305, United States, [⊥]Energy and Environmental Directorate, Pacific Northwest National Laboratory, 902 Battelle Boulevard, Richland, Washington 99352, United States, [¶]Stanford Institute for Materials and Energy Sciences, SLAC National Accelerator Laboratory, 2575 Sand Hill Road, Menlo Park, California 94025, United States, and [∇]National Renewable Energy Laboratory, 1617 Cole Boulevard, Golden, Colorado 80401, United States. [†]These authors contributed equally to this paper.

ABSTRACT Silicon (Si)-based materials hold promise as the next-generation anodes for high-energy lithium (Li)-ion batteries. Enormous research efforts have been undertaken to mitigate the chemo-mechanical failure due to the large volume changes of Si during lithiation and delithiation cycles. It has been found that nanostructured Si coated with carbon or other functional materials can lead to significantly improved cyclability. However, the underlying mechanism and comparative performance of different coatings remain poorly understood. Herein, using *in situ* transmission electron microscopy (TEM) through a nanoscale half-cell battery, in combination with chemo-mechanical simulation, we explored the effect of thin (~5 nm) alucone and Al₂O₃ coatings on the lithiation kinetics of Si nanowires (SiNWs). We observed that the alucone coating leads to a “V-shaped” lithiation front of the SiNWs, while the Al₂O₃ coating yields an “H-shaped” lithiation front. These observations indicate that the difference between the Li surface diffusivity and bulk lithiation rate of the coatings dictates lithiation induced morphological evolution in the nanowires. Our experiments also indicate that the reaction rate in the coating layer can be the limiting step for lithiation and therefore critically influences the rate performance of the battery. Further, the failure mechanism of the Al₂O₃ coated SiNWs was also explored. Our studies shed light on the design of high capacity, high rate and long cycle life Li-ion batteries.



KEYWORDS: Silicon nanowire · lithium ion battery · surface coating · *in situ* TEM

Silicon (Si) has been identified as a promising candidate as the next-generation anode material for lithium (Li)-ion batteries (LIBs) because of its high Li storage capacity (~3579 mAh/g) achieved with Li₁₅Si₄ as the final phase at room temperature.^{1–3} However, Si undergoes large volume changes (~300%) during lithiation/delithiation process, causing disintegration of active anode materials from the battery system.^{4–7} To address this issue inherent to Si-based anodes, nanostructuring and compositing with carbon or other functional materials^{7–25} have been widely explored to improve the electrochemical

performance of Si-based anodes. In particular, surface coatings^{26–36} on nanoparticles (NPs) or nanowires (NWs), rather than a simple mixture of conductive additives and Si, received considerable attention, and have been proven to be an effective way to enhance the cycling performance. Surface coatings are expected to function in multiple roles: First, they act as a protective layer that can mitigate the unwanted and continuous side reactions between Si and electrolytes. Second, a conductive coating layer can ensure good electronic and/or ionic contact during cycling. Third, the coating layer acts as a mechanical confinement

* Address correspondence to
suz10@psu.edu,
Chunmei.Ban@nrel.gov,
Chongmin.Wang@pnnl.gov.

Received for review March 18, 2015
and accepted April 20, 2015.

Published online April 20, 2015
10.1021/acsnano.5b01681

© 2015 American Chemical Society

that buffers the volume change of the anode during cycling.

Carbonaceous materials, such as amorphous carbon and graphite, are excellent candidate coating materials due to their high conductivity and high mechanical strength. These properties yield improved structural stability, cyclability and coulombic efficiency of Si.²⁶ Other types of coatings were also explored. Atomic layer deposition (ALD) of Al₂O₃ coatings on cathodes has been reported as a protective layer by preventing the cathodes from side reactions with the electrolyte.^{28,37} Similarly, an ALD Al₂O₃ coating on Si anodes^{31,32} was used as an artificial solid electrolyte interphase (SEI) layer to suppress the decomposition of electrolytes caused by surface reactions on Si. Recently, it has been shown that organic–inorganic composite layers deposited *via* molecular layer deposition (MLD) can effectively tailor the mechanical properties and the electronic and ionic conductivities of Si-based anodes.³⁸ Specifically, the MLD process can eliminate the native oxide layer on Si particles, leading to fast lithiation and high Coulombic efficiency.^{11,39} Though several types of coatings have been demonstrated to improve the Si anode performance, the underlying mechanisms remain elusive. From a design perspective, it is vital to understand how the surface coatings evolve structurally and chemically during the electrochemical cycling, and how such structural and chemical evolutions affect the lithiation/delithiation kinetics and degradation of Si anodes.

Herein, we use a half-cell nanobattery coupled with *in situ* transmission electron microscopy (TEM) to characterize the lithiation behavior of Si nanowires (SiNWs) with two types of surface coatings: Al₂O₃ and MLD alucone. Our studies show that the difference in the surface diffusion relative to the bulk lithiation of the two types of coatings gives rise to distinct lithiation morphologies. We further observed the intimate coupling between lithiation kinetics and stress generation and failure in the surface coated SiNWs, which sheds light on the rational design of durable Si-based anode materials.

RESULTS AND DISCUSSIONS

Figure 1A,C shows the high-resolution (HR) TEM images of the morphologies of alucone and Al₂O₃ coated SiNWs, featuring conformal surface coatings with a thickness of ~5 nm. Both the alucone and Al₂O₃ coating layers show strong adhesion to the SiNWs. The chemical compositions of coating layer for both alucone and Al₂O₃ were analyzed using energy dispersive X-ray spectroscopy (EDXS) in scanning transmission electron microscopy (STEM), as shown in Figure 1, panels B and D, respectively. The Al and O are rich on the surface of the Al₂O₃ coated SiNWs (panel D), indicating a uniform Al₂O₃ layer was deposited. The C and O are rich in the region of alucone coating (panel B),

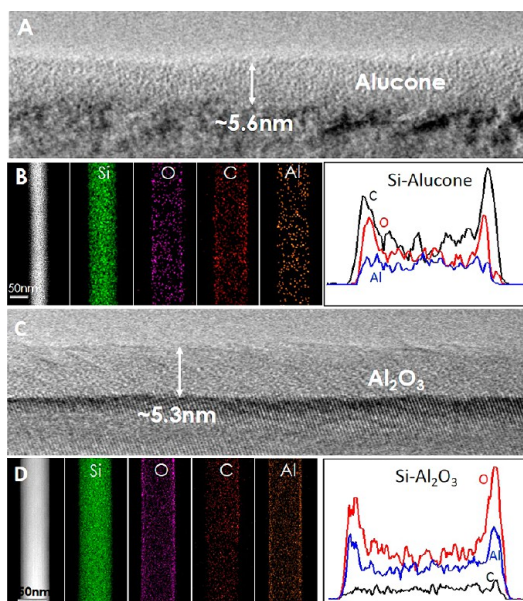


Figure 1. (A and C) Bright-field TEM images of conformal coatings of alucone and Al₂O₃ on Si nanowires. (B and D) STEM mode energy dispersive X-ray spectroscopy (EDXS) elemental mapping and cross-sectional elemental profile of alucone (C and O rich in the coating region) and Al₂O₃ (Al and O rich in the coating region) coated Si nanowire, respectively.

indicating that Al-polymer composite (3D network of $-Al_n(-OCH_2-CHO-CH_2O)_m$ ($n:m = 1$)) is coated.

The initial lithiation process of alucone coated SiNWs is illustrated by a series of time-resolved TEM images captured from Supporting Information Video S1. Prior to lithiation, the SiNW had a uniform diameter of ~160 nm, as shown in Figure 2A. After a bias of -3 V was applied, Li ions were electrochemically driven from Li₂O/Li (the bottom) to alloy the alucone coated SiNW. The lithiation proceeded by the migration of the two-phase interface separating the crystalline Si (*c*-Si) phase and lithiated amorphous Li_{*x*}Si (*a*-Li_{*x*}Si) phase, which has been revealed as the typical lithiation mechanism for *c*-Si materials.⁷ Lithiation first caused notable radial expansion in the region close to the electrode/electrolyte contact point, as highlighted by the white arrows in the bottom. The lithiation depth decreased gradually from the contact point to the far in the longitudinal direction, exhibiting a “V-shaped” lithiation front, as shown in Figure 2B,C. Throughout the lithiation process, the alucone coating layer remained morphologically intact and tightly bonded with the SiNW, as shown in Figure 2E,F, though the coating thickens from 4 to 10 nm.

Another interesting observation from Figure 2A–C is the lithiation process for a small alucone coated Si nanoparticle (SiNP) (~45 nm) that attached to a coated SiNW (~160 nm). As indicated by the top white arrow, the coated SiNP is lithiated with Li ions supplied *via* their surface diffusion along the SiNW since the SiNP is far from the Li₂O electrolyte. We observed that the size

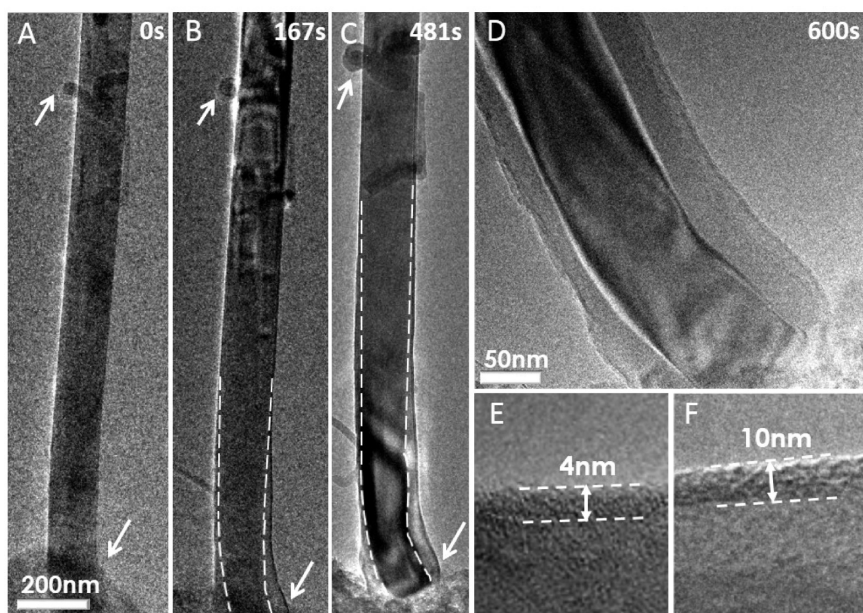


Figure 2. (A–C) Time-resolved TEM images of an alucone-coated SiNW under lithiation. White dash lines indicate the interface that separates lithiated and unlithiated regions. (D) Magnified view of the close end of SiNW after 600s lithiation; TEM images of alucone coatings before (E) and after (F) lithiation.

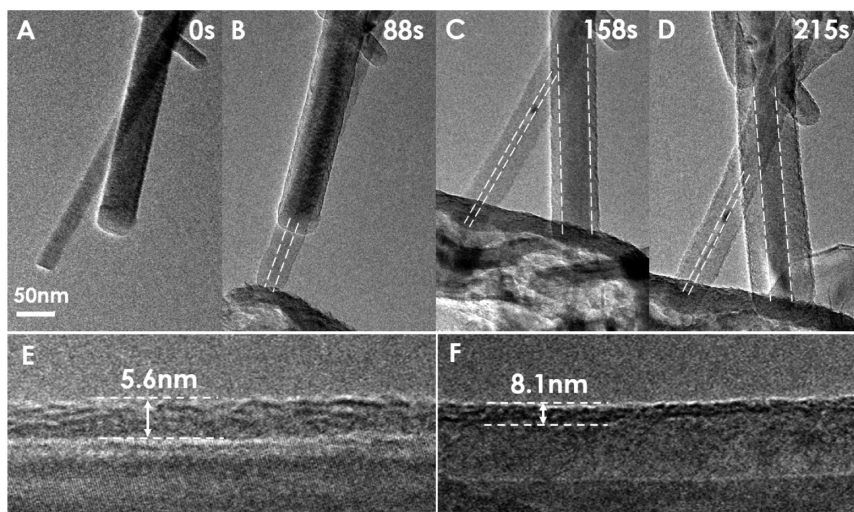


Figure 3. (A–D) Time-resolved bright-field TEM images of an Al_2O_3 -coated SiNW under lithiation, with white dash lines indicating the interface between lithiated and unlithiated regions; TEM images of the alucone coatings before (E) and after (F) lithiation.

of Si nanostructures plays a vital role in the lithiation kinetics. The smaller the size of the nanostructures, the larger the surface-to-volume ratio they have. Thus, for smaller nanostructures, the fraction of surface lithiation is larger, and lithiation is faster. The large surface-to-volume ratio also relaxes the lithiation-generated stress more effectively.^{40,41} Both lead to a faster lithiation rate in smaller sized nanostructures. We observed that the SiNP was nearly fully lithiated in 300 s ($\sim 300\%$ volume expansion), while the adjacent part of SiNW was barely lithiated, consistent with the size-dependent lithiation kinetics.

Figure 3 depicts a series of time-resolved TEM images of the lithiation process of two Al_2O_3 coated

SiNWs (see the Supporting Information Video S2). As shown from Figure 3A,B, only the thinner (pristine, ~ 26 nm in diameter) SiNW was in direct contact to the $\text{Li}_2\text{O}/\text{Li}$, and after ~ 40 s its diameter grew to 44 nm, corresponding to a $\sim 286\%$ volume expansion assuming no longitudinal expansion. Although the thicker (pristine, ~ 52 nm in diameter) SiNW was not in direct contact with $\text{Li}_2\text{O}/\text{Li}$, it became lithiated and its diameter reached 61 nm ($\sim 161\%$ volume expansion), as shown in Figure 3B, possibly due to the contact between the two SiNWs. As shown in Figure 3C,D, the second period of lithiation started at 158 s with both SiNWs in contact with the $\text{Li}_2\text{O}/\text{Li}$. We observed that the thicker SiNW grew from 61 to 91 nm in diameter

in 60 s, while the thinner one only expanded 2 nm in diameter during this time period, as shown in Figure 3C,D. Lithiation over the two time periods resulted in a total volume expansion of $\sim 316\%$ and $\sim 306\%$ for the thin and thick SiNWs, respectively. The faster lithiation of the less lithiated SiNW in the second period is possible due to the lithiation-induced stress effect. It has been revealed that lithiation induces compressive stress at the reaction front, causing a retardation effect on further lithiation. As lithiation depth increases, lithiation-induced compressive stress at the reaction front also increases, and the retardation effect becomes stronger.^{38,42–44} This explains lithiation proceeds faster in less lithiated SiNWs. We further observed that during the whole lithiation process of both two Al_2O_3 coated SiNWs the thicknesses of the lithiated layers increased evenly along the longitudinal direction of the nanowires over time, exhibiting an “H-shaped” lithiation front. After lithiation, Al_2O_3 coating remained on the Si surface, as shown in Figure 3E,F. The thickness of the coating increased from 5.6 to 8.1 nm, indicating the Al_2O_3 layer was also lithiated.

We compare the lithiation kinetics of alucone and Al_2O_3 coated SiNWs with the same diameter to eliminate the size effect on lithiation kinetics. As shown in Figure 4, the time-resolved TEM images in panels A and B depict the typical lithiation process for the alucone and Al_2O_3 coated SiNWs with the same diameter, respectively. The alucone coated SiNW has a clear “V-shaped” lithiation front, comparing to the “H-shaped” lithiation front of the Al_2O_3 coated SiNW as shown in the corresponding schematic drawings. Figure 4C displays the lithiation depth vs time for the two types of SiNWs, showing that lithiation proceeds much faster in the alucone coated SiNW. This is consistent with our previous results on the alucone coated SiNPs that have a supreme fast lithiation/delithiation rate.³⁸ The linearity of the curves also indicates that lithiation in the coated SiNWs is reaction limited.

The distinct lithiation front profiles in alucone (“V-shaped”) and Al_2O_3 (“H-shaped”) coated SiNWs may stem from the difference in the relative reaction rate of Li on the surface and in the bulk for these two coatings. Generally, surface lithiation is diffusion limiting, and is much faster than the bulk lithiation, which is reaction limiting. We denote $\alpha = (k_s/k_b)$, the ratio of the surface (k_s) and bulk (k_b) lithiation rates, where $\alpha \gg 1$. The self-limiting effect of lithiation due to the lithiation-induced compressive stress at the reaction front further slows down the reaction rate, or equivalently a smaller k_b , giving rise to an even larger α . Similar to the native SiO_2 layer on bare SiNWs, Al_2O_3 coatings have a low intrinsic Li ion conductivity and high mechanical stiffness (and hence high compressive stress at the lithiation front). Thus, the stress-mediated Li reaction rate within the Al_2O_3 coating is much slower

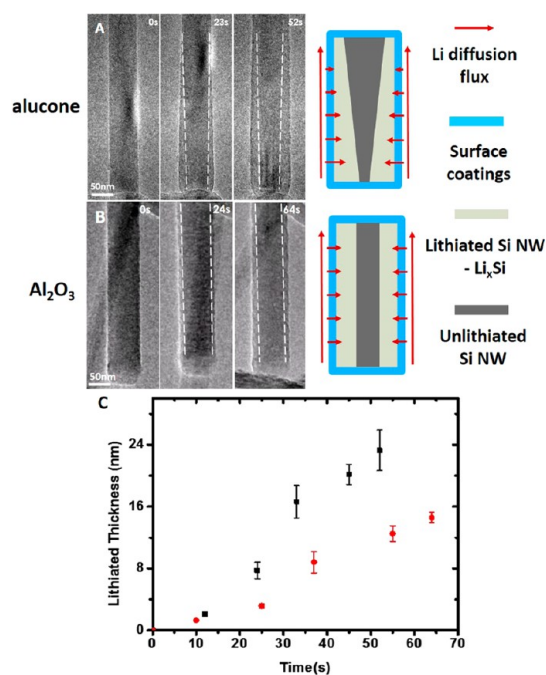


Figure 4. (A and B) Time-resolved TEM images show the development of lithiation profiles of the alucone and Al_2O_3 coated SiNWs and schematics of the Li diffusion paths through the SiNWs that dictate the lithiation behavior; (C) average lithiation thickness vs time for the alucone (black square) and Al_2O_3 (red dot) coated SiNWs.

than its surface diffusion on the Al_2O_3 coatings. In contrast, because of the high Li permeability, the intrinsic Li reaction rate in bulk alucone is relatively higher. Lithiation generated compressive stress at the reaction front is also low because of its low stiffness. We follow $\alpha_{\text{Al}_2\text{O}_3} \gg \alpha_{\text{alucone}}$. Thus, in Al_2O_3 coated SiNWs, Li quickly covers the surface of the coating before appreciable radial lithiation occurs. In fact, any point of the same radial position along the axial direction of the nanowire is lithiated nearly at the same time, resulting an “H-shaped” lithiation front, as shown in Figure 4B. The similar lithiation profile was also observed in bare SiNWs.⁴² In contrast, because α_{alucone} is relatively small (though still much larger than 1), lithiation along the radial direction within the alucone coating close to the Li source is appreciable while lithium quickly covers the surface of the coating, resulting in a “V-shaped” lithiation front, as shown in Figure 4A.

To further elucidate the surface coating mediated lithiation kinetics of SiNWs, we employ a chemomechanical model that couples Li transport and stress generation to simulate the lithiation process.^{43,45} In our simulations, the surface and bulk diffusivities are set to be 100 and 0.5, respectively, in the alucone coatings, and 1000 and 0.001 in the Al_2O_3 coatings. The relative rates are $\alpha_{\text{alucone}} = 200$, and $\alpha_{\text{Al}_2\text{O}_3} = 10^6$. Li diffusivity in Si is set to be 0.001. Figure 5 displays the morphologies of the partially lithiated SiNWs with these two types of coatings at three different lithiation states, which agree very well with the experimental observations.

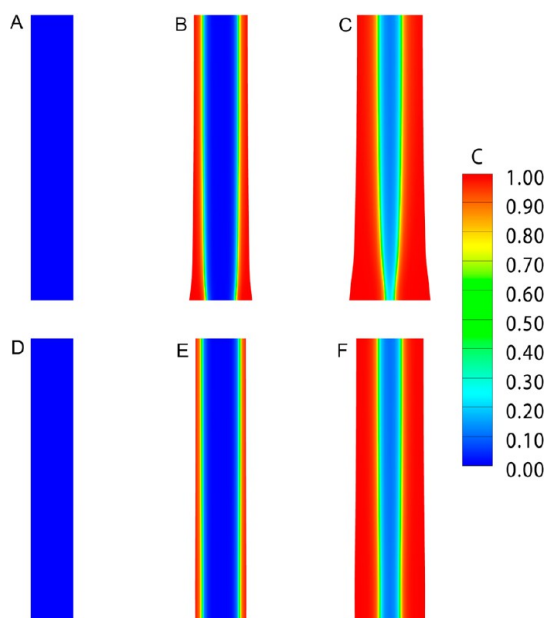


Figure 5. Chemo-mechanical modeling of the lithiation processes of the alucone and Al_2O_3 coated SiNWs. For better visualizing the processes, only the Li distribution on cross sections of the nanowires are shown, with red color indicating the fully lithiated phase and blue the unlithiated phase. (A–C) Lithiation of an alucone coated SiNW. (D–F) Lithiation of an Al_2O_3 coated SiNW. (A and D) Pristine SiNWs with different coatings before lithiation. (B and E) Lithiation process starts from the bottom ends of the SiNWs. (C and F) Partially lithiated SiNWs. The low intrinsic Li ion conductivity of the Al_2O_3 coating layer results in an “H-shaped” lithiation front, while the high Li permeability of the alucone layer leads to a “V-shaped” lithiation front.

As mentioned above, the Al_2O_3 coating or native oxide layer on Si has a low intrinsic Li ion conductivity, resulting in accumulation of a large amount of Li ions on the surface when charging the Si electrode. Because a large electrochemical driving force is required to lithiate this type of coating, much higher than that required for Si alloying with Li, it could induce pulverization of Si nanostructures or damage to functional surface coatings. This phenomenon is illustrated in the bright-field TEM images in Figure 6, captured from Supporting Information Video S3. In particular, an Al_2O_3 coated SiNW is pulverized and broke into half along its twin boundary when lithiated. NWs No. 1 and 2 are in direct contact with $\text{Li}_2\text{O}/\text{Li}$, while No. 3 NW is in contact with both 1 and 2 on the upper side and lower side, respectively, as shown in Figure 6A. Upon biasing, the No. 1 and 2 NWs were quickly lithiated to reach the maximum volume expansion ($\sim 300\%$) within 23 s because of their small dimensions and short diffusion path. At the same time, No. 3 NW was slowly lithiated with its diameter increased from 100.2 to 105.1 nm after 23 s as shown in Figure 6B. After full lithiation of No. 1 and 2 NWs, the No. 3 NW started to be lithiated at a much faster rate with its diameter increased from 105.1 to 140.2 nm in another 25 s shown in Figure 6C. However, this steady lithiation process was

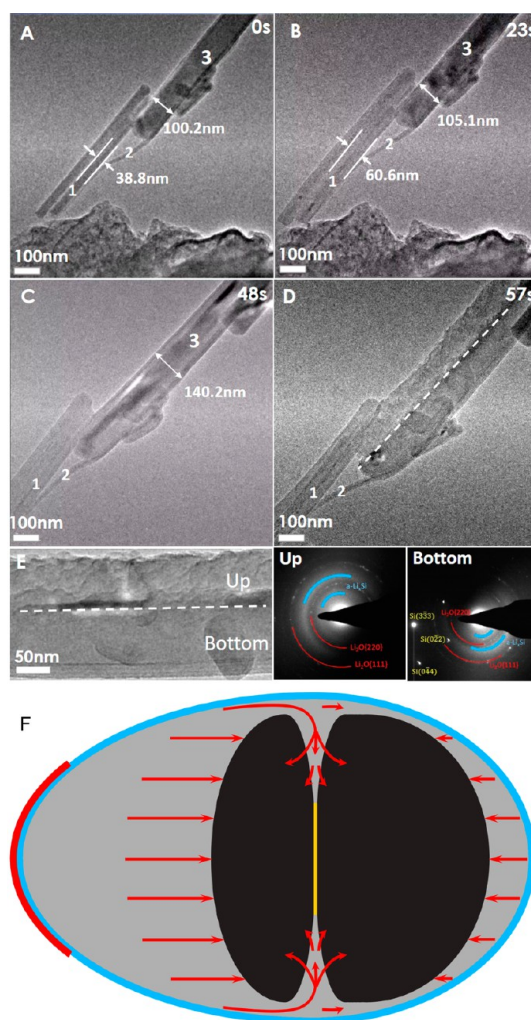


Figure 6. (A–D) Time sequential TEM images of the failure process of an Al_2O_3 coated SiNW. (E) Enlarged TEM image of the No.3 SiNW divided into upper and bottom half and corresponding electron diffraction patterns. The upper half is fully amorphized, while the lower half is only partially lithiated, manifesting the asymmetry of lithiation kinetics. (F) A schematic showing symmetry breaking in lithiation kinetics that results in pulverization of the SiNW. Red arrows represent the Li flow; Li sources on the outer surface is indicated by red, lithiated coating layer by cyan, lithiated amorphous shell by gray, unlithiated Si core by black, and the twin boundary by yellow.

interrupted by sudden pulverization of the upper half followed by the separation of the two halves (Figure 6D). Electron diffraction patterns (Figure 6E) of the pulverized SiNW show that the upper half was completely lithiated and amorphized, while the lower half was only partially lithiated with an unlithiated crystalline core.

The asymmetric pulverization of the Al_2O_3 coated SiNW is likely due to the asymmetric lithiation kinetics and the presence of the twin boundary between the upper and lower halves of the SiNW, as schematically shown in Figure 6F. Once the No. 1 and No. 2 SiNWs are fully lithiated, they become more conductive than the pristine state. Since the No. 1 SiNW is thicker than the No. 2 SiNW, the upper surface of the No. 3 SiNW is more supersaturated by Li ions than the lower surface.

Under a large overpotential (-3 V), the Al_2O_3 coating in the upper half is fully lithiated before the lower half. The fully lithiated coating in the upper part then serves as a fast lithium transport channel for further lithiation. The fast lithium flow stream branches into the lower half and the twin boundary.⁴⁶ As this lithiation continues, the upper half of SiNW becomes fully lithiated while the lower half is only partially lithiated. Owing to the large volume expansion and stress generated in the upper half as well as the weak twin boundary, the coating breaks, and the upper half of the SiNW pulverizes and separates from the lower half, while the lower half of the SiNW remains structurally intact. This phenomenon was not observed in lithiation of alucone coated SiNWs, possibly because the permeable alucone coating allows smoother Li ion diffusion and the lithiated coating is mechanically more flexible. The above observation indicates the importance of surface modifications in regulating lithiation kinetics and damage control in Si-based anodes.

It should be pointed out that the electrode/electrolyte interface in the current open-cell configuration is different from that in real batteries. For the case of a real battery, the SiNWs are fully immersed in the liquid electrolyte, forming a conformal coating and therefore Li ion can diffuse in from all directions. Accordingly, the "V-shaped" lithiation profile observed for alucone coated SiNWs may be absent in real battery. For the *in situ* open-cell, the Li source is in contact with one end of the SiNW, which appears to be distinctively different from

the real situation, but it is just this open-cell configuration that uniquely offers us the opportunity of probing the effect of the coating layer on Li ion diffusion. Therefore, the intrinsic structural change (core-shell mode) and the effect of coatings on the lithiation kinetics of SiNWs are well presented for real batteries.

CONCLUSIONS

In summary, the effects of two types of surface coatings, alucone and Al_2O_3 , were investigated on the lithiation behavior of SiNWs. Lithiation in these two coatings and Si are reaction limiting. The difference in the Li surface diffusivity relative to the bulk lithiation rate in these two coatings gives rise to distinctly different lithiation morphologies: an "H-shaped" reaction front in Al_2O_3 coated SiNWs and a "V-shaped" alucone coated SiNWs. Our experiments also demonstrate the intimate coupling between lithiation kinetics and stress generation. Lithiation proceeds much faster in less lithiated SiNWs, possibly due to the lower compressive stress at the reaction front, and hence weaker lithiation retardation effect. The asymmetric lithiation kinetics in the Al_2O_3 coated SiNWs results in asymmetric pulverization of the SiNW. The surface coating effect on the lithiation behavior of SiNWs revealed in our studies provides insights on the surface structural and chemical modifications of Si nanostructured anodes for enhanced battery performance.

METHODS

Fabrication of the SiNW and processing of the coating layer have been reported in prior papers.^{11,39} The structure and chemical composition of coating layers were examined by high-resolution transmission electron microscopy (HRTEM) imaging and energy dispersive X-ray spectroscopy analysis (EDXS). The EDXS mapping was carried on a JEOL ARM-200 coupled with Si drift detector. HRTEM images and *in situ* TEM images were acquired using Titan 80-300 fitted with an objective lens image corrector and operated at 300 kV.

The *in situ* TEM observation of the lithiation and delithiation of the nanowires was carried out using an open-cell configuration as schematically illustrated in Supporting Information Figure S1. The silicon nanowires were loaded on Pt rod, which is fixed on one side of TEM holder (Nanofactory STM). Lithium metal is loaded on W rod which is navigated by piezoelectric system on the other side of the holder. Lithium metal is driven to contact the silicon particles. The lithium oxide layer on lithium metal surface serves as electrolyte. To drive Li^+ diffusion in Li_2O , an overpotential of -3 V is applied on Si against the Li metal to lithiate the Si. The microstructure changes were recorded using a charge-couple device (CCD) attached to the TEM.

Conflict of Interest: The authors declare no competing financial interest.

Acknowledgment. This work at PNNL, NREL, and Stanford is supported by the Assistant Secretary for Energy Efficiency and Renewable Energy, Office of Vehicle Technologies of the U.S. Department of Energy under Contract No. DE-AC02-05CH11231, Subcontract No. 18769 and DE-AC-36-08GO28308 under the Advanced Batteries Materials Research. The *in situ* microscopic study described in this paper is supported by the

Laboratory Directed Research and Development Program as part of the Chemical Imaging Initiative at Pacific Northwest National Laboratory (PNNL). The work was conducted in the William R. Wiley Environmental Molecular Sciences Laboratory (EMSL), a national scientific user facility sponsored by DOE's Office of Biological and Environmental Research and located at PNNL. PNNL is operated by Battelle for the DOE under Contract DE-AC05-76RLO1830. H.Y. and S.L.Z. acknowledge the support by the NSF-CMMI (Grant No. 0900692).

Supporting Information Available: Description of the material. This material is available free of charge via the Internet at <http://pubs.acs.org>.

REFERENCES AND NOTES

1. Kasavajjula, U.; Wang, C. S.; Appleby, A. J. Nano- and Bulk-Silicon-Based Insertion Anodes for Lithium-Ion Secondary Cells. *J. Power Sources* **2007**, *163*, 1003–1039.
2. Obrovac, M. N.; Christensen, L. Structural Changes in Silicon Anodes during Lithium Insertion/Extraction. *Electrochem. Solid-State Lett.* **2004**, *7*, A93–A96.
3. Kubota, Y.; Escaño, M. C. S.; Nakanishi, H.; Kasai, H. Crystal and Electronic Structure of $\text{Li}_{15}\text{Si}_4$. *J. Appl. Phys.* **2007**, *102*, 053704.
4. Lee, S. W.; McDowell, M. T.; Berla, L. A.; Nix, W. D.; Cui, Y. Fracture of Crystalline Silicon Nanopillars during Electrochemical Lithium Insertion. *Proc. Natl. Acad. Sci. U.S.A.* **2012**, *109*, 4080–4085.
5. Liu, X. H.; Wang, J. W.; Huang, S.; Fan, F.; Huang, X.; Liu, Y.; Krylyuk, S.; Yoo, J.; Dayeh, S. A.; Davydov, A. V.; et al. *In Situ* Atomic-Scale Imaging of Electrochemical Lithiation in Silicon. *Nat. Nanotechnol.* **2012**, *7*, 749–756.

6. Liu, X. H.; Zheng, H.; Zhong, L.; Huang, S.; Karki, K.; Zhang, L. Q.; Liu, Y.; Kushima, A.; Liang, W. T.; Wang, J. W.; et al. Anisotropic Swelling and Fracture of Silicon Nanowires during Lithiation. *Nano Lett.* **2011**, *11*, 3312–3318.
7. Liu, X. H.; Zhang, L. Q.; Zhong, L.; Liu, Y.; Zheng, H.; Wang, J. W.; Cho, J.-H.; Dayeh, S. A.; Picraux, S. T.; Sullivan, J. P.; Mao, S. X.; et al. Ultrafast Electrochemical Lithiation of Individual Si Nanowire Anodes. *Nano Lett.* **2011**, *11*, 2251–2258.
8. Dimov, N.; Kugino, S.; Yoshio, M. Carbon-Coated Silicon as Anode Material for Lithium Ion Batteries: Advantages and Limitations. *Electrochim. Acta* **2003**, *48*, 1579–1587.
9. Green, M.; Fielder, E.; Scrosati, B.; Wachtler, M.; Moreno, J. S. Structured Silicon Anodes for Lithium Battery Applications. *Electrochem. Solid-State Lett.* **2003**, *6*, A75–A79.
10. Dimov, N.; Kugino, S.; Yoshio, M. Mixed Silicon–Graphite Composites as Anode Material for Lithium Ion Batteries: Influence of Preparation Conditions on the Properties of the Material. *J. Power Sources* **2004**, *136*, 108–114.
11. Chan, C. K.; Peng, H.; Liu, G.; Mcllwraith, K.; Zhang, X. F.; Huggins, R. A.; Cui, Y. High-Performance Lithium Battery Anodes Using Silicon Nanowires. *Nat. Nanotechnol.* **2008**, *3*, 31–35.
12. Hu, Y. S.; Demir-Cakan, R.; Titirici, M. M.; Muller, J. O.; Schlogl, R.; Antonietti, M.; Maier, J. Superior Storage Performance of a Si@SiO₂/C Nanocomposite as Anode Material for Lithium-Ion Batteries. *Angew. Chem., Int. Ed.* **2008**, *47*, 1645–1649.
13. Kim, H. J.; Han, B. H.; Choo, J. B.; Cho, J. Three-Dimensional Porous Silicon Particles for Use in High-Performance Lithium Secondary Batteries. *Angew. Chem., Int. Ed.* **2008**, *47*, 10151–10154.
14. Lee, Y. J.; Lee, Y.; Oh, D.; Chen, T.; Ceder, G.; Belcher, A. M. Biologically Activated Noble Metal Alloys at the Nanoscale: For Lithium Ion Battery Anodes. *Nano Lett.* **2010**, *10*, 2433–2440.
15. Song, T.; Xia, J.; Lee, J.; Lee, D.; Kwon, M.; Choi, J.; Wu, J.; Doo, S.; Chang, H.; Park, W.; et al. Arrays of Sealed Silicon Nanotubes as Anodes for Lithium Ion Batteries. *Nano Lett.* **2010**, *10*, 1710–1716.
16. Evanoff, K.; Magasinski, A.; Yang, J. B.; Yushin, G. Nano-silicon-Coated Graphene Granules as Anodes for Li-Ion Batteries. *Adv. Energy Mater.* **2011**, *1*, 495–498.
17. Yao, Y.; McDowell, M. T.; Ryu, I.; Wu, H.; Liu, N.; Hu, L.; Nix, W. D.; Cui, Y. Interconnected Silicon Hollow Nanospheres for Lithium-Ion Battery Anodes with Long Cycle Life. *Nano Lett.* **2011**, *11*, 2949–2954.
18. Chen, X. L.; Li, X. L.; Ding, F.; Xu, W.; Xiao, J.; Cao, Y. L.; Meduri, P.; Liu, J.; Graff, G. L.; Zhang, J. G. Conductive Rigid Skeleton Supported Silicon as High-Performance Li-Ion Battery Anodes. *Nano Lett.* **2012**, *12*, 4124–4130.
19. Gowda, S. R.; Pushparaj, V.; Herie, S.; Girishkumar, G.; Gordon, J. G.; Gullapalli, H.; Zhan, X.; Ajayan, P. M.; Reddy, A. L. M. Three-Dimensionally Engineered Porous Silicon Electrodes for Li Ion Batteries. *Nano Lett.* **2012**, *12*, 6060–6065.
20. Li, X. L.; Meduri, P.; Chen, X. L.; Qi, W.; Engelhard, M. H.; Xu, W.; Ding, F.; Xiao, J.; Wang, W.; Wang, C. M.; et al. Hollow Core-Shell Structured Porous Si-C Nanocomposites for Li-Ion Battery Anodes. *J. Mater. Chem.* **2012**, *22*, 11014–11017.
21. Luo, J.; Zhao, X.; Wu, J.; Jang, H. D.; Kung, H. H.; Huang, J. Crumpled Graphene-Encapsulated Si Nanoparticles for Lithium Ion Battery Anodes. *J. Phys. Chem. Lett.* **2012**, *3*, 1824–1829.
22. Wu, H.; Zheng, G.; Liu, N.; Carney, T. J.; Yang, Y.; Cui, Y. Engineering Empty Space between Si Nanoparticles for Lithium-Ion Battery Anodes. *Nano Lett.* **2012**, *12*, 904–906.
23. Chang, J.; Huang, X.; Zhou, G.; Cui, S.; Hallac, P. B.; Jiang, J.; Hurley, P. T.; Chen, J. Multilayered Si Nanoparticle/Reduced Graphene Oxide Hybrid as a High-Performance Lithium-Ion Battery Anode. *Adv. Mater.* **2014**, *26*, 758–764.
24. Jeong, G.; Kim, J.-G.; Park, M.-S.; Seo, M.; Hwang, S. M.; Kim, Y.-U.; Kim, Y.-J.; Kim, J. H.; Dou, S. X. Core–Shell Structured Silicon Nanoparticles@TiO₂-x/Carbon Mesoporous Microfiber Composite as a Safe and High-Performance Lithium-Ion Battery Anode. *ACS Nano* **2014**, *8*, 2977–2985.
25. Li, X.; Gu, M.; Hu, S.; Kennard, R.; Yan, P.; Chen, X.; Wang, C.; Sailor, M. J.; Zhang, J.-G.; Liu, J. Mesoporous Silicon Sponge as an Anti-Pulverization Structure for High-Performance Lithium-Ion Battery Anodes. *Nat. Commun.* **2014**, *5*, 4105.
26. Yoshio, M.; Wang, H.; Fukuda, K.; Umeno, T.; Dimov, N.; Ogumi, Z. Carbon-Coated Si as a Lithium-Ion Battery Anode Material. *J. Electrochem. Soc.* **2002**, *149*, A1598–A1603.
27. Yen, Y.-C.; Chao, S.-C.; Wu, H.-C.; Wu, N.-L. Study on Solid-Electrolyte-Interphase of Si and C-Coated Si Electrodes in Lithium Cells. *J. Electrochem. Soc.* **2009**, *156*, A95–A102.
28. Jung, Y. S.; Cavanagh, A. S.; Dillon, A. C.; Groner, M. D.; George, S. M.; Lee, S.-H. Enhanced Stability of LiCoO₂ Cathodes in Lithium-Ion Batteries Using Surface Modification by Atomic Layer Deposition. *J. Electrochem. Soc.* **2010**, *157*, A75–A81.
29. Scott, I. D.; Jung, Y. S.; Cavanagh, A. S.; Yan, Y.; Dillon, A. C.; George, S. M.; Lee, S.-H. Ultrathin Coatings on Nano-LiCoO₂ for Li-Ion Vehicular Applications. *Nano Lett.* **2010**, *11*, 414–418.
30. Seok Jung, Y.; Cavanagh, A. S.; Yan, Y.; George, S. M.; Manthiram, A. Effects of Atomic Layer Deposition of Al₂O₃ on the Li[Li_{0.20}Mn_{0.54}Ni_{0.13}Co_{0.13}]O₂ Cathode for Lithium-Ion Batteries. *J. Electrochem. Soc.* **2011**, *158*, A1298–A1302.
31. Xiao, X.; Lu, P.; Ahn, D. Ultrathin Multifunctional Oxide Coatings for Lithium Ion Batteries. *Adv. Mater.* **2011**, *23*, 3911–3915.
32. Nguyen, H. T.; Zamfir, M. R.; Duong, L. D.; Lee, Y. H.; Bondavalli, P.; Pribat, D. Alumina-Coated Silicon-Based Nanowire Arrays for High Quality Li-Ion Battery Anodes. *J. Mater. Chem.* **2012**, *22*, 24618–24626.
33. Han, X.; Liu, Y.; Jia, Z.; Chen, Y.-C.; Wan, J.; Weadock, N.; Gaskell, K. J.; Li, T.; Hu, L. Atomic-Layer-Deposition Oxide Nanogluer for Sodium Ion Batteries. *Nano Lett.* **2013**, *14*, 139–147.
34. Zhang, X.; Belharouak, I.; Li, L.; Lei, Y.; Elam, J. W.; Nie, A.; Chen, X.; Yassar, R. S.; Axelbaum, R. L. Structural and Electrochemical Study of Al₂O₃ and TiO₂ Coated Li_{1.2}Ni_{0.13}Mn_{0.54}Co_{0.13}O₂ Cathode Material Using ALD. *Adv. Energy Mater.* **2013**, *3*, 1299–1307.
35. Wu, H.; Chan, G.; Choi, J. W.; Ryu, I.; Yao, Y.; McDowell, M. T.; Lee, S. W.; Jackson, A.; Yang, Y.; Hu, L. B.; Cui, Y. Stable Cycling of Double-Walled Silicon Nanotube Battery Anodes through Solid-Electrolyte Interphase Control. *Nat. Nanotechnol.* **2012**, *7*, 309–314.
36. Sandu, G.; Brassart, L.; Gohy, J.-F.; Pardoën, T.; Melinte, S.; Vlad, A. Surface Coating Mediated Swelling and Fracture of Silicon Nanowires during Lithiation. *ACS Nano* **2014**, *8*, 9427–9436.
37. Cho, J.; Kim, Y. J.; Park, B. Novel LiCoO₂ Cathode Material with Al₂O₃ Coating for a Li Ion Cell. *Chem. Mater.* **2000**, *12*, 3788–3791.
38. He, Y.; Piper, D. M.; Gu, M.; Travis, J. J.; George, S. M.; Lee, S.-H.; Genc, A.; Pullan, L.; Liu, J.; Mao, S. X.; Zhang, J.-G.; Ban, C.; Wang, C. *In Situ* Transmission Electron Microscopy Probing of Native Oxide and Artificial Layers on Silicon Nanoparticles for Lithium Ion Batteries. *ACS Nano* **2014**, *8*, 11816–11823.
39. Piper, D. M.; Travis, J. J.; Young, M.; Son, S.-B.; Kim, S. C.; Oh, K. H.; George, S. M.; Ban, C.; Lee, S.-H. Reversible High-Capacity Si Nanocomposite Anodes for Lithium-ion Batteries Enabled by Molecular Layer Deposition. *Adv. Mater.* **2014**, *26*, 1596–1601.
40. Chan, C. K.; Peng, H. L.; Liu, G.; Mcllwraith, K.; Zhang, X. F.; Huggins, R. A.; Cui, Y. High-Performance Lithium Battery Anodes Using Silicon Nanowires. *Nat. Nanotechnol.* **2008**, *3*, 31–35.
41. Liu, X. H.; Zhong, L.; Huang, S.; Mao, S. X.; Zhu, T.; Huang, J. Y. Size-Dependent Fracture of Silicon Nanoparticles during Lithiation. *ACS Nano* **2012**, *6*, 1522–1531.

42. Liu, X. H.; Fan, F.; Yang, H.; Zhang, S.; Huang, J. Y.; Zhu, T. Self-Limiting Lithiation in Silicon Nanowires. *ACS Nano* **2013**, *7*, 1495–1503.
43. Yang, H.; Fan, F.; Liang, W.; Guo, X.; Zhu, T.; Zhang, S. A Chemo-mechanical Model of Lithiation in Silicon. *J. Mech. Phys. Solids* **2014**, *70*, 349–361.
44. Yang, H.; Liang, W.; Guo, X.; Wang, C.-M.; Zhang, S. Strong Kinetics-Stress Coupling in Lithiation of Si and Ge Anodes. *Extreme Mech. Lett.* **2015**, *2*, 1–6.
45. Yang, H.; Huang, S.; Huang, X.; Fan, F.; Liang, W.; Liu, X. H.; Chen, L.-Q.; Huang, J. Y.; Li, J.; Zhu, T.; Zhang, S. Orientation-Dependent Interfacial Mobility Governs the Anisotropic Swelling in Lithiated Silicon Nanowires. *Nano Lett.* **2012**, *12*, 1953–1958.
46. Gu, M.; Yang, H.; Perea, D. E.; Zhang, J.-G.; Zhang, S.; Wang, C.-M. Bending-Induced Symmetry Breaking of Lithiation in Germanium Nanowires. *Nano Lett.* **2014**, *14*, 4622–4627.